Toxic and Physiological Metal Uptake and Release by Human Serum Transferrin

David J. Reilley,[‡] Jack T. Fuller III,[‡] Michael R. Nechay,[‡] Marie Victor,[‡,§] Wei Li,[‡,‖] Josiah D. Ruberry,[‡] Jon I. Mujika,[⊥] Xabier Lopez,[⊥] and Anastassia N. Alexandrova[*,‡,¶]

‡*Department of Chemistry and Biochemistry, University of California, Los Angeles, 607 Charles E. Young Drive East, Los Angeles, CA 90095-1569, USA*

§*Institut Lumire Matire, 10 rue Ada Byron, 69622 Villeurbanne CEDEX, France*

‖*Department of Chemistry and Chemical Biology, Harvard University, 12 Oxford Street, Cambridge, MA 02138*

⊥*Kimika Fakultatea, Euskal Herriko Unibertsitatea (UPV/EHU) and Donostia International Physics Center, PK 1072, 20080 Donostia, Euskadi, Spain*

¶*California NanoSystems Institute, University of California, Los Angeles, 570 Westwood Plaza, Los Angeles, California 90095-1569, USA*

E-mail: ana@chem.ucla.edu

Phone: +1 310 8253769

Running header

Metal Transport by Human Serum Transferrin

Abstract

An atomistic understanding of metal transport in the human body is critical to anticipate the side effects of metal-based therapeutics and holds promise for new drugs and drug delivery designs in itself. Human serum transferrin (hTF) is a central part of the transport processes with its ubiquitous ferrying of physiological Fe(III) and other transition metals, including to tightly controlled parts of the body. There is an atomistic mechanism for the uptake process with Fe(III), but not for the release process or for other metals. This study provides initial insight into these processes for a range of transition metals (Ti(IV), Co(III), Fe(III), Ga(III), Cr(III), Fe(II), Zn(II)) through fully atomistic, extensive QM/DMD sampling and a new technique we developed to calculate relative binding affinities between metal cations and the protein. It identifies protonation of Tyr188 as a trigger for metal release, rather than protonation of Lys206 or Lys296. The study identifies difficulty of metal release from hTF as potentially related to cytotoxicity. Simulations identify a few critical interactions that stabilize the metal-binding site in a flexible, nuanced manner.

Statement of Significance

Human serum transferrin (hTF) is a Fe(III) transport protein that may be implicated in the cytotoxicity of non-native metals like Ti(IV), Ga(III), and Al(III). However, hTF transport and especially release are not well studied for metals beyond Fe(III). In this study we computationally investigate the uptake and release mechanisms and affinities for a range of transition metals (Ti(IV), Co(III), Fe(III), Ga(III), Cr(III), Fe(II), Zn(II)). We find that the tightest binding metals of this list are Ti(IV) and Ga(III): the potentially cytotoxic ones.

Introduction

Human serum transferrin (hTF) is of medical interest for its unique role in toxic metal pathology. The protein natively carries atomic iron into the cell from blood by receptor-mediated endocytosis. However, it is believed to also competitively transport other transition metals based on *in vitro* binding studies, including Ti(IV), Co(III), Ga(III), Cr(III), and Al(III).(*1–3*) While some of these metals, namely Co(III), may be necessary for homeostasis in the appropriate concentrations, others (including Ti(IV) and Al(III)) are believed to exhibit some degree of cytotoxicity even at low concentrations.(*4*, *5*) Ti(IV) in particular can bind to DNA as well as inhibit various intracellular enzymes.(*6*, *7*) The ability of hTF to transport toxic metals is therefore of great concern with the increasing bioavailability of these metals due to modern industry and their medical applications.(*5*, *8–10*) This is acutely problematic as the protein could bring these metals to sensitive parts of the body by its ability to pass the blood-brain barrier as well as concentrate them in cancer cells due to the over expression of the transferrin receptor across a range of tumors.(*11*, *12*) Though troubling, these abilities have been providing unique oppertunities to develop new anticancer drugs and drug delivery techniques to the brain based on hTF or its receptor.(*13–15*) Ultimately, a thorough structural understanding of hTF and how it binds and transports a variety of transition metals can improve knowledge of their toxicology as well guide the development of novel drugs and new tools for drug delivery.

The basic biological activity and structure of hTF are well characterized. It is a member of the transferrin family of glycoproteins, which regulate free iron concentration in physiological fluids such as blood by hTF, milk and tears by lactoferrin, and egg whites by ovotransferrin. hTF is a 80 kDa protein comprised of two domains, termed the N- and C-domains, each containing a pair of highly similar subdomain lobes connected by a hinge. Each domain can bind an iron ion with a synergistic anion (typically carbonate) near the hinge between its two lobes (Figure 1).(*16*) When hTF binds two iron atoms, it is recognized by transferrin receptor 1 and the entire protein is brought into the cell by endocytosis.(*17*) The change

from the blood serum pH (7.4) to the lower pH of the endosomes (5.6) then triggers the release of iron from hTF.(*18*)

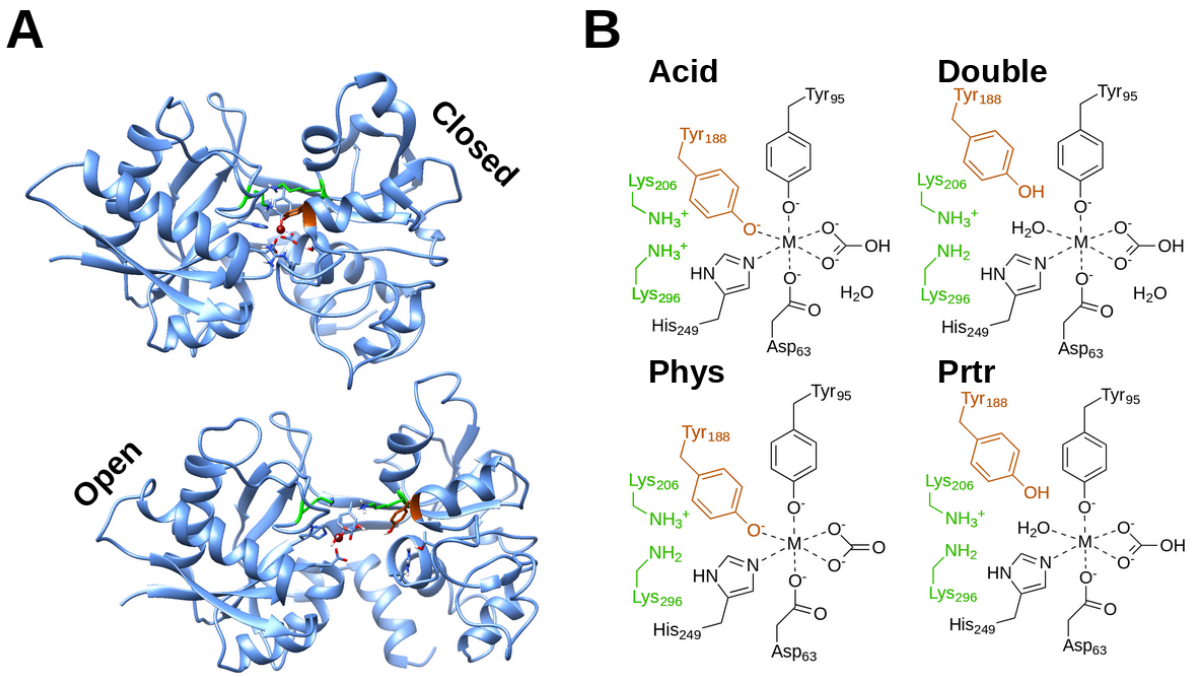

Figure 1: (A) Examples of open and closed hTF N-domain conformers with iron (in red) loaded in the active site between two lobes. The closed form comes from a diferric bound crystal structure (PDB ID: 3V83) at blood serum pH, and the open form comes from a computationally generated structure from this study. (B) The hTF active site in four different protonation states considered in our calculations based on structures from the reference 27. According to that study, the Phys and Acid forms yield closed conformers while the Double and Prtr forms, with Tyr188 protonated, become open. The difference between the Double and Prtr structures is the inclusion of an additional explicit water molecule in the active site of the Double form. In both parts of this figure, the dilysine bridge is in bright green while Tyr188 is in dark orange.

The mechanism of hTF binding and releasing iron and other metals is not fully understood despite extensive study, and further clarification poses particular challenges for experimental approaches. A large body of work, including native PAGE gels, small angle X-ray scattering, X-ray absorption fine structure spectroscopy (XAFS) and crystal structures, suggest the protein undergoes a hinging conformational change between the lobes in each domain from a closed state at physiological pH to an open one at endosomal pH.(*19*, *20*) This is believed to facilitate iron capture and release by protecting and then exposing the

active site to solvent. There are a few possible chemical triggers for this action which may operate in conjunction or separately, including metal reduction(*21*) and protonation of specific residues. In the N-domain, the better studied of the two, the conformational change was long thought to be driven primarily by a dilysine bridge: a pair of interacting lysines (Lys206 and Lys296), one from each lobe, where the lower pH protonates and breaks this interaction.(*22*) However, while mutagenesis studies did indicate that the bridge is important for proper hTF activity,(*23*) there is no experimental confirmation of the exact role it plays. The necessary, direct, structural inspection of the open forms of hTF is hampered by their embedding in the cellular machinery of endocytosis. Some crystal structures have been obtained with hTF in a receptor-bound state or at low pH,(*24*, *25*) but it is difficult to capture the effect of both conditions on structure and dynamics.(*26*) Only two crystal structures (PDB ID: 5DYH, 5H52) demonstrate a truly open conformation beyond a few degrees of interlobal twisting.(*27*, *28*) However, both use the larger citrate as a synergistic anion and were obtained in blood serum uptake, rather than endosomal release, conditions. These issues have made further study into the release activity of hTF difficult to pursue with experiment alone. The release mechanism is unknown at a structural level and even its basic kinetics (akin to references 1 and 2) across all metals is simply unstudied.

Past computational studies have filled in and revised the structural and mechanistic details of the hTF metal transport mechanism, but these are not yet complete. Crystal structures of two mutants to the dilysine bridge first suggested that breaking this interaction alone fails to trigger the conformational change.(*29*) Later molecular dynamics studies by the Lopez group,(*30*) based on a hypothesis from Rinaldo and Field,(*31*) showed that protonation of a tyrosine that coordinates the metal (Tyr188) prompts the conformational change regardless of the protonation state of the dilysine bridge. The simulations found this behavior present for both native Fe(III) and Al(III). These results, however, were based mainly on force field based molecular dynamics, which has severe limitations for the appropriate treatment of transition metals. Moreover, previous QM/MM MD simulations at the

semi-empirical level coupled with DFT/MM minimizations(*32*) for Fe(III) and Al(III) suggested the importance of introducing a quantum method to fully characterize the interaction mode of these two cations with the surrounding ligands.

This study aims to investigate the atomistic root for the hinging phenomenon in the N-domain of hTF with extensive QM/DMD simulations and consider how this mode of binding and release might vary for a range of transition metals. QM/DMD is a rapid sampling method for metalloenzymes (described thoroughly in the Theoretical Methods section) that can treat the chemistry of the bound metal and its coordination quantum mechanically. In addition, we describe a new method to evaluate the relative binding affinites of the metals to hTF in all its forms at both uptake and release. Besides Fe(III), we performed simulations with metals necessary for the human body, Fe(II), Co(III), Cr(III), and Zn(II), and increasingly bioavailable non-native metals that may have acute cytotoxicity, Ti(IV) and Ga(III). We conducted the simulations on four different protonation states derived from reference 27: the physiological form found in blood serum (Phys), the protein with just the dilysine bridge protonated (Acid), and the protein with Tyr188 protonated and either one or two additional water ligands to the metal (PrTr and Double respectively) (Figure 1). The Phys and Acid forms are hypothesized to be closed, while the Double and Prtr forms are open and likely implicated in metal release into the endosome. The results show a remarkable structural similarity across all considered metals with some subtle differences in transient interactions about the active site that may explain their relative affinities to hTF, ability to undergo uptake and release, and implications for metal toxicity.

Theoretical Methods

A total of 5 replicate QM/DMD trajectories were run for each metal for each form of the protein for a total of 140 simulations. Each trajectory corresponds roughly to 20 ns of simulation. Full rationalization and details about the preparation of each system can be

found in the supplementary information (SI).

These simulations were performed with the established QM/DMD method.(*33*) This is a technique for sampling metalloprotein conformations using quantum mechanical (QM) electronic structure calculations necessary to model the metal and its coordination (referred to as the 'QM region') and discrete molecular dynamics (DMD)(*34*) to describe the rest of the protein. Both methods treat an overlapping QM/DMD region, consisting of species participating in important, non-covalent interactions near the metal, to enable inter-region communication and mitigate discontinuity errors. QM/DMD has a strong record of successfully explaining a variety of metalloenzyme behaviors. These include metal-dependent catalytic activity,(*35–38*) protein metal affinity,(*35*) sequence and cofactor-dependent redox functionality,(*33*, *39*) the role of protein electrostatics in activity,(*40*) effect of mutagenesis on structure,(*33*, *41*, *42*) and flexible docking to metalloenzymes.(*43*)

All QM calculations in this study were performed at the DFT level of theory with Turbomole (version 6.6).(*44*) The pure meta-GGA TPSS functional(*45*) was used with the D3 dispersion correction.(*46*) The metal was treated with the triple-zeta basis set def2-TZVPP and all other atoms with the double-zeta def2-SVP basis set.(*47*) While the small basis set may result in some degree of basis set superposition error, the large size of the QM regions have precluded the use of larger basis sets. Furthermore, the level of theory employed has proven effective in the past studies, cited above, including for quantitative free energy comparisons. Finally, the Conductor-like Screen Model (COSMO) with a constant dielectric of 4 was applied to approximate the screening and solvation effects in the relatively buried active sites of the systems.(*48*) Water molecules which coordinate to the metal were modeled explicitly. The QM calculations were performed to convergence within 1.0×10^{-7} Hartree or at least 100 SCF cycles. This approach enhances sampling and plotting the energy trajectories shows most QM calculations are close to convergence by this point. All DMD phases in the iterative QM/DMD simulations in this study were performed for 10,000 steps per iteration (0.5 ns). DMD runs with an implicit solvent through appropriate potentials in its forcefield.

Convergence of the QM/DMD simulations was achieved according to a series of benchmarks. These consist of the protein backbone RMSD (calculated with respect to the alpha carbon and amide carbon, nitrogen, and oxygen of each amino acid), the DMD energy, and QM energy. The RMSD values were calculated with the initial protein equilibrated for one QM/DMD iteration as the reference structure. The backbone RMSD trajectories of each system are included in this text as an example (Figure 2), while charts of the other two metrics can be found in the supporting information.

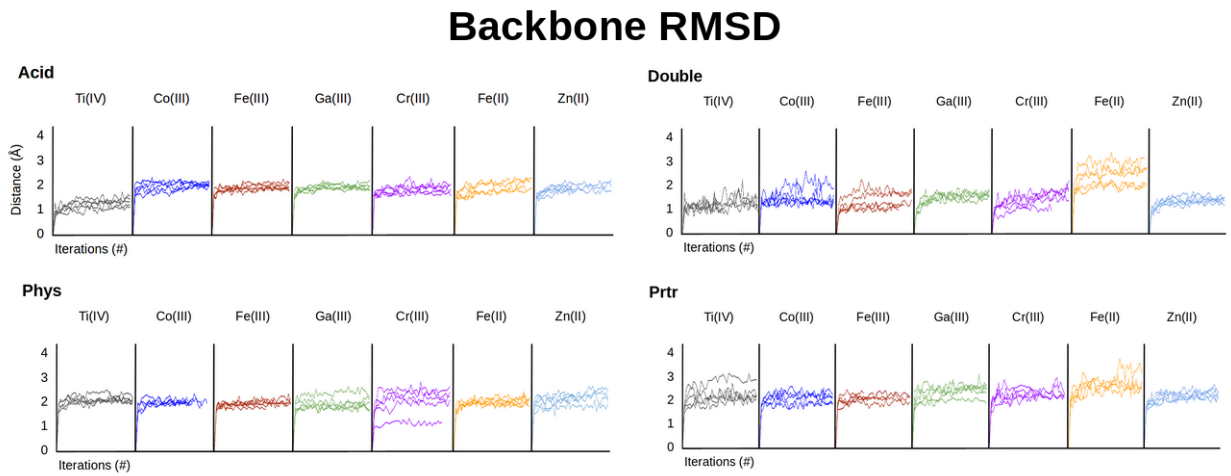

Figure 2: Plots of the backbone RMSD by timestep for every QM/DMD simulation in this study. The plots group all replicates by metal: Ti(IV) (grey), Co(III) (deep blue), Fe(III) (red), Ga(III) (green), Cr(III) (purple), Fe(II) (gold), Zn(II) (light blue) for each protein protonation form: Acid, Phys, Double, Prtr. Most replicates oscillate around the value of 2 Å indicating convergence. The open forms of the protein (Double and Prtr) report more variations from this value befitting their greater flexibility, especially with Fe(II), but still show convergence in each case.

The spin state for each metal was estimated and then verified so that the best was used to generate the data for this study. Geometry optimizations with DFT at the same level of theory as described for QM/DMD were performed on each feasible spin multiplicity for each metal in the acid form of hTF. The spin state of the optimized structure with the lowest electronic energy for each metal was then used for the appropriate QM/DMD simulations. After the simulations were completed, all reasonable spin multiplicities were tested for the lowest energy structure from each trajectory of the acid forms of the most suspect metals:

Fe(II), Fe(III), Cr(III), and Co(III). Fe(II), Fe(III), and Cr(III) were found to be high-spin, and Co(III) was found to be low-spin. The QM/DMD simulations for these metals were rerun with the corrected spin-states as necessary.

All computational binding affinities in this study were calculated by a new, relative approach.(*35*) A direct approach would involve computing free energies of the metal ion in solution, the apo-protein, and the metal-containing protein. However, the free energy of a metal cation in water is highly dependent on the local structure of water and therefore ill-defined. Furthermore, a metalloenzyme in its apo-form can be prone to unfolding or refolding and so assessing its free energy becomes prohibitively expensive. Instead, the new method uses EDTA-metal complexes as an intermediate step in a thermodynamic cycle (Figure 3). This cycle captures the energy of the unbound metal in the experimentally derived metal-EDTA binding energy and leaves the tractable terms of EDTA-protein transition to calculation. However, to fully cancel the EDTA terms, the approach can only calculate relative affinities between different metals within the same form of hTF.

The calculation of the relative binding affinities required just some data on EDTA besides information from the QM/DMD simulations. Experimental values for the free energy of binding of each metal to EDTA were obtained from a database.(*49*) The free energy calculation for each of the EDTA-metal complexes started with a DFT geometry optimization with the same software and at nearly the same level of theory used in QM/DMD. The only differences are that COSMO was given a dielectric of 84 corresponding to the water solvent and each optimization was run out to total convergence. The free energy was then calculated from the optimized geometry with a harmonic frequency calculation with the same settings. As Ti(IV) is missing experimental EDTA binding data, an additional step was included in the cycle for this metal using experimentally available data on Ti(III). The sum of aqueous redox potential of Ti(IV) to Ti(III),(*50*, *51*) the Ti(III)-EDTA binding energy, and the computed difference between the Ti(III)-EDTA and Ti(IV)-EDTA complexes yields an EDTA binding energy for Ti(IV).

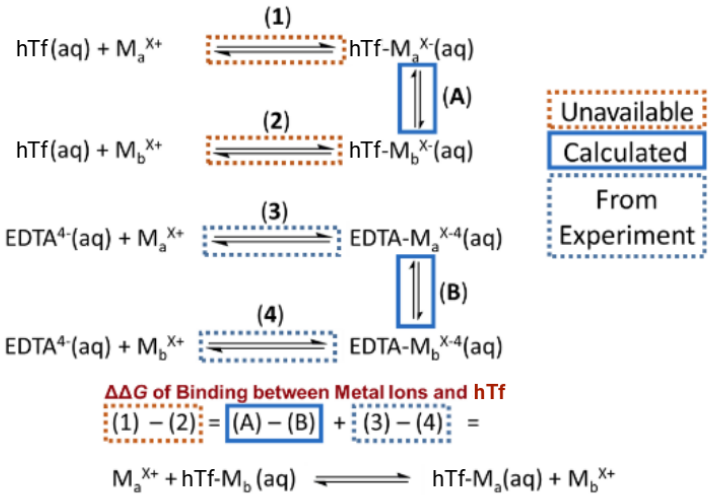

Figure 3: Thermodynamic cycle for the relative affinity of metal binding to hTF. The parenthesized label next to each box around an equilibrium process corresponds to the free energy of that tranistion. The desirable processes (1) and (2) are intractable as the structure of free metal ions in solution is not defined (dashed red boxes). The new method in this study provides the free energy associated with the chemical reaction at the bottom. It is calculated as the sum of the difference between processes (3) and (4) which utilize available, experimental data for EDTA-metal binding (dashed blue boxes). This is summed with the difference between processes (A) and (B) which capture metal exchange (solid blue boxes). The result is a G that reconstructs the difference between processes (1) and (2): the difference between the binding affinities of the metals.

Further optimization of the QM region was done to generate the structures for free energy and metal angle variance calculations. This was done on the lowest lying unoptimized QM regions for each metal in each form of the protein. First, the three lowest electronic energy structures were optimized. The average deviation in the drop in electronic energy they experienced was taken. All unoptimized QM/DMD structures within two standard deviations of the lowest unoptimized structure were then selected for full optimization. Each set of structures were optimized to full convergence and free energies were calculated for them by a harmonic frequency calculation at the same level of theory and with the same software as above. Of these the structure with the lowest free energy was then selected as the representative minimum for its structure of the protein and metal.

Results and Discussion

Interlobal distances calculated from the QM/DMD simulations confirm the role of Tyr188 as the switch controlling the functional hTF conformational transition. The interlobal distance was calculated as the smallest distance between two sets of residue alpha carbons that define the two sides of the central binding pocket (Figure 4). One set consists of residues 12-14, 43-46, 290, and 291 while the other is comprised of residues 179-182. When the interlobal distance was determined for each iteration of all simulations, it shows that the Acid and Phys forms of the protein maintain a distance of about 5 Å while the Double and Prtr forms vary over their trajectories but rarely shrink below 10 Å (Figure 5). The 5 Å distance corresponds to a closed conformation and any distance above that corresponds to an open conformation. This demonstrates that the forms of the protein with Tyr188 deprotonated stay closed, regardless of the protonation state of the dilysine bridge (as this is protonated in the closed Acid form); the forms with Tyr188 protonated by contrast generally stay open but occasionally approach a closed state in Ti(IV) and Fe(II) Double. The simulations therefore corroborate the results of reference 27 on the role of Tyr188 over the dilysine bridge and

shows that the open forms of the protein are more flexible.

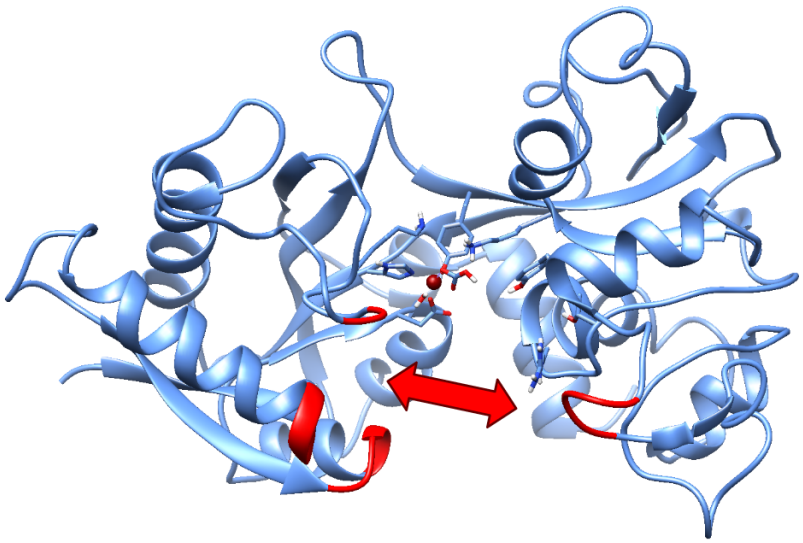

Figure 4: The interlobal distance was measured between the alpha carbon of the red loops opposite each other on the hTF cleft.

The calculated relative free energies of metal-hTF binding qualitatively match experimental results. To calculate these free energy differences, we utilized the relative binding affinity approach described in the Theoretical Methods section. The most significant drawback to this approach is that the free energy of binding must be calculated relative to another metal. This is still a valuable and vetted technique: when applied to the lowest energy structures from the QM/DMD simulations with physiological Fe(III) as reference the results can be qualitatively compared to in vitro binding affinities. In fact, the experimental order determined and estimated in references 1 and 2 closely matches the order of the relative free binding energies calculated for the Phys form, the dominant structure in the experimental conditions (Table 1). The observed differences are for metals with similar enough experimental and estimated affinities and theoretical free energies to agree within an acceptable margin of error (due to abberations in the experimental setup and computational techniques). Only Ti(IV), Co(III), Cr(III) deviate significantly, and the experimental values for Co(III) and Cr(III) are suspect as they were extrapolated from binding constants to small molecules rather than directly measured.(*1*) This concurrence supports our methods for the

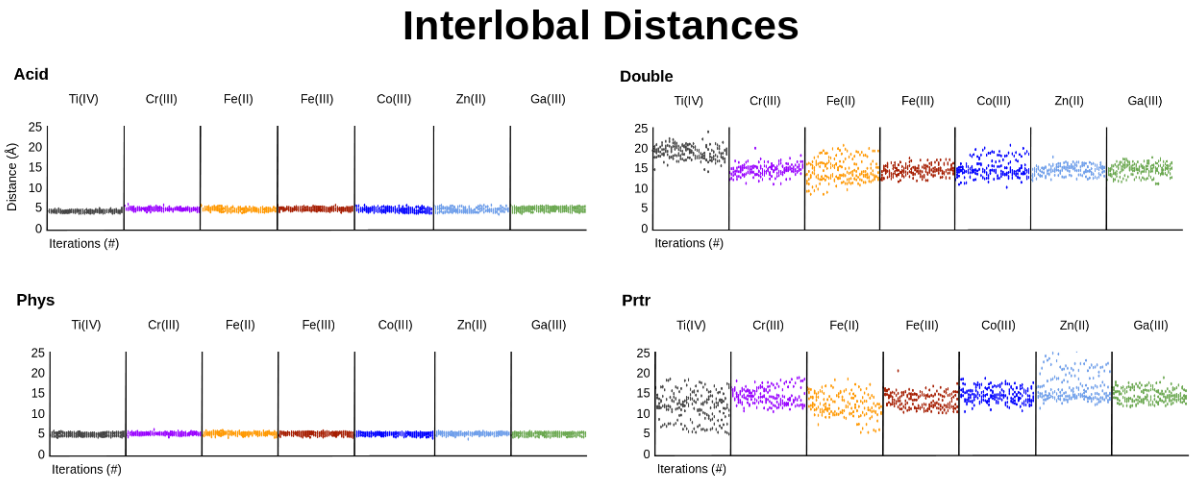

Figure 5: Plots of the interlobal distance for each form of the protein and each metal. The distance is recorded as a scatter plot with all replicates overlaid. These plots show that, regardless of metal, the Acid and Phys forms of the protein maintain a closed conformation for all metals with an interlobal distance of about 5 Å while the Double and Prtr forms typically stay open with distances consistently higher.

calculation of the relative free energies of binding and what they say about hTF activity.

Table 1: Table of the experimental(*1*, *2*) and calculated relative binding affinities to the N-terminal domain of hTF each sorted by metal in descending order. The experimental affinities reported as ranges (Co(III) and Cr(III)) were estimated. The energies are relative to their respective unscaled values of Fe(III), which correspondingly have values of 0 kcal/mol.

Exp. (kcal/mol)	Ti(IV): -5.8	Co(III): -2.0 to +1.9	Fe(III): 0	Ga(III): 2.6	Cr(III): 4.1 to 8.2	Fe(II): 20.1	Zn(II): 21.4
Calc. (kcal/mol)	Ti(IV): -56.5	Co(III): -14.8	Fe(III): 0	Ga(III): -3.3	Cr(III): 0.0	Fe(II): 26.4	Zn(II): 20.0

The order of the relative free energies of binding provides unique insight into the potential of various metals to compete with physiological Fe(III) for hTF — insight which could distinguish cytotoxic from healthy behavoir. As the chemistry of the active site is slightly different between the forms of the protein, relative free energies can't be calculated across the open to closed forms. However, comparisons can be made relative to Fe(III) for each state (Figure 6). As established above, the calculated binding free energies in the Phys form of the protein describe how well each metal is uptaken by hTF from solution akin to blood serum. Given the mechanistic role of the open conformers of hTF, orders for these forms of the protein correspondingly suggest how well each metal is released in conditions similar to the endosome. Our calculations therefore divide the metals into three categories based on

how well they bind in the closed and open forms of hTF: (1) those that don't compete with Fe(III), (2) those that do, and (3) those that could outcompete Fe(III) for hTF. The first category comprises divalent metals Fe(II) and Zn(II). These metals bind worse than Fe(III) in both conformational states and therefore do not compete for hTF as they are uptaken poorly and released readily. The second category is composed of Co(III), Cr(III). These metals, in contrast, can be transported by hTF as they bind better than Fe(III) in the Phys form but worse in the open forms of the protein. The final category may include Ti(IV) and Ga(III), which could interfere in natural hTF behavior. They bind better than Fe(III) in the Phys form, but according to the Double form of the protein are released about as easily as the physiological metal. Whether Ti(IV) and Ga(III) are in the second or third category is dependent on whether the Double of Prtr form is more mechanistically relevant as these disagree on the release potential of these metals. Note that these two metals are the non-essential and potentially cytotoxic ones in our study, so sequestering hTF could be related to their toxicity and merits future investigation. This is particularly important for Ti(IV) with its immense predicted affinity for the protein. As our study suggests that Co(III), Cr(III), and especially Ti(IV) and Ga(III) all compete with Fe(III) in hTF activity, it is important to understand the structural underpinning for this.

The structural analysis of the QM/DMD simulations focuses on the active site, which varies the most with the generally subtle effect of different metals. Considered here are the metal angle variance and distance of critical hydrogen bonding interactions. Consistent with the observations from the interlobal distances, these analyses demonstrate that the closed Acid and Phys forms of hTF are rigid and do not significantly change over the course of the QM/DMD simulations, while the open Double and Prtr forms are flexible. However, the analyses do not identify a single interaction or property that distinguish individual metal binding preferences. Instead, the order of metal binding affinities arises from an ensemble of critical interactions implicated in hTF metal transport behavior.

The metal angle variance simply matches chemical intuition and does not correlate with

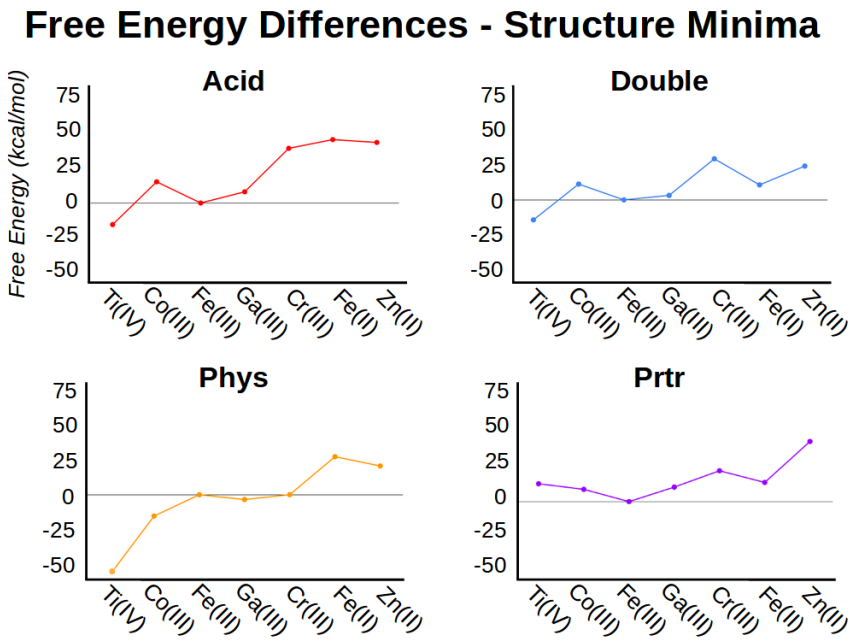

Figure 6: Free energies of binding relative to Fe(III) for each metal and form of hTF. Notice the marked difference in metal binding preferences across the four forms. These were all calculated for the fully optimized, lowest energy QM regions from the QM/DMD simulations.

the binding free energies. This is a measurement of how much the geometry of the metal deviates from the ideal octahedral. It arises from the equation: $\sigma^2_{oct} = \frac{1}{11}\sum_{i=1}^{12}(\theta_i - 90°)^2$ which sums the difference of each of the 12 characteristic angles of an octahedral geometry from the ideal 90° (Figure 7). The metal angle variance was calculated for the optimized, lowest energy structure of each metal and protein form (Figure 8). The divalent metals Fe(II) and Zn(II) are the only ones to consistently deviate from octahedral, which makes sense as they generally prefer a tetrahedral geometry. Indeed, both of these metals typically reject a ligand to adopt a coordination closer to this geometry over the course of their QM/DMD simulations, in agreement with previous calculations by Sakajiri et al. (*52*). Otherwise, just Ti(IV) and Fe(III) vary a small amount from the baseline in open forms of the protein. Ultimately, the results further demonstrate the greater flexibility of the open forms of the protein, but do not identify a direct structural correlation to the free energy of binding besides the intuitive poor binding performance of the divalent metals.

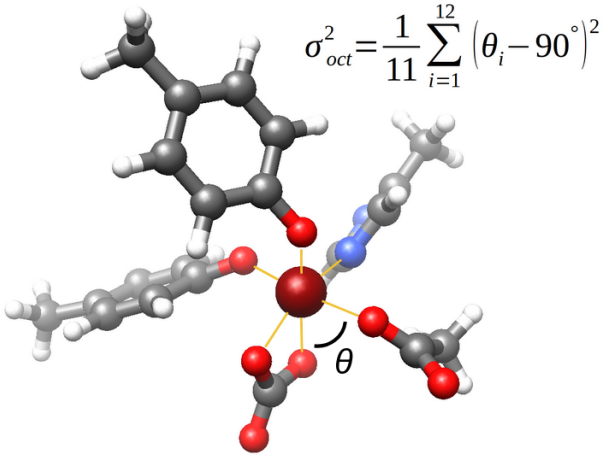

Figure 7: Example metal geometry in the hTF active site; the twelve angles used to calculate the metal angle variance are defined between each pair of adjacent ligand bonds (solid gold lines).

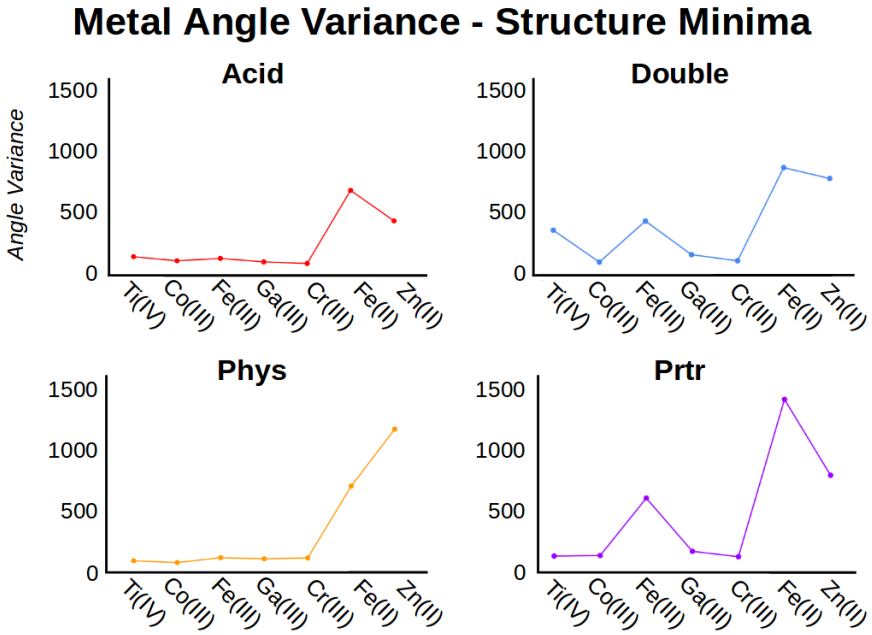

Figure 8: Metal angle variances calculated for each metal and form of the protein. Notice how only the divalent metals and occasionally Ti(IV) and Fe(III) deviate significantly from the low values and therefore octahedral geometries. As with the calculated relative binding free energies, these were calculated for just the fully optimized, lowest energy QM regions from the QM/DMD simulations.

There are a number of critical, hydrogen-bonding interactions around the active site that vary significantly between metals and forms of the protein, but no single interaction directly correlates with the binding free energies across all systems (Figures 9). This makes sense if we consider that the roles of the secondary hydrogen-bonding interactions around the active site are to keep the active site residues in the optimimum arrangement, while the electrostatic interactions of the residues coordinating to the metal most directly affect relative binding energy. Note that relatively good qualitative results were obtained in a previous study for the binding affinity in the Phys state by considering only first-shell residues provided that these are fixed at their corresponding active site positions.(*52*) Regardless, the characterization of the hydrogen-bonding interactions around the active site is important to at least understand the relevant interactions in the stabilization of the structure of the metal-binding site. Therefore, we have made a thorough analysis of the important, most varying interactions. For each of them, the smallest distance between potential atomic partners was recorded for each timestep of each relevant simulation. The data were summed over intervals of 1 Å and plotted as smoothed histograms by protein form with all metals color-coded and overlaid (Figures 10). The first set of distances considered here are between the synergistic carbonate anion and its hydrogen bonding partners on Arg124, Ser125, Tyr188. These graphs show that as the protein transitions from its closed to the open forms, Arg124 generally moves away from the characteristic hydrogen-bonding distance of 2.5 Å while Ser125 and Tyr188 generally move towards it. These residues therefore take over the role of stabilizing the carbonate from Arg124. This is consistent with observations made in reference 27, which saw Arg124 as an indicator of protein conformational change. Another highly varying distance is between hydrogen bonding partners on Asp292 and the water ligand found in the open conformers. The histograms show that this interaction is only present in the Prtr form, and is only preferred to a significant degree in the Co(III), Ti(IV), Fe(III), and Zn(II) forms of the protein. This interaction in particular has effects which extend out of the active site, as Asp292 adopting it tugs on the loop comprised of residues 289-294 and

changes its shape. Ultimately, these interactions vary significantly between metals, but none individually correlate with the calculated free energies. Instead, it is the composite of these interactions and the electrostatic interactions with first-shell residues which explains hTF behavior.

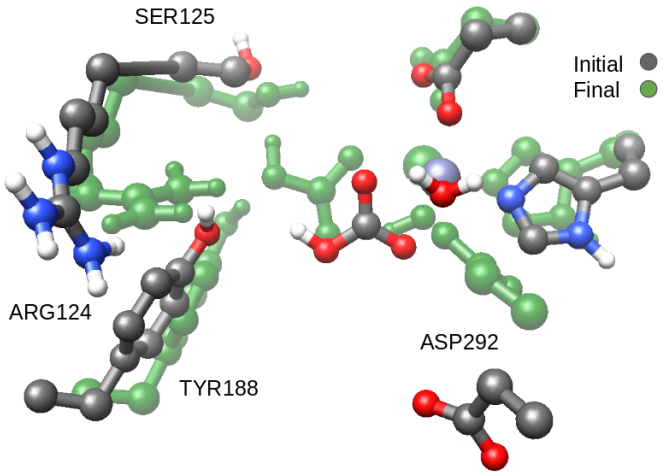

Figure 9: Overlay of two exemplary active sites (both of the Prtr form, with gray from a briefly equilibrated structure and green from a structure toward the end of a simulation) from the QM/DMD simulations demonstrating the possible range of motion. The structures show how the Asp292-water distance and interactions between the carbonate anion and Arg124, Ser125, Tyr188 are flexible.

Conclusion

The atomistic insight QM/DMD simulations provide into the hTF uptake and release process shows that cytotoxic metals can successfully compete with Fe(III) in transport and may get trapped in the protein, but are hard to target as the only observed differences are small and nuanced. The simulations confirm that the conformational hinging which drives hTF metal transport is fundamental to each of the considered metals beyond just Fe(III). Furthermore, for all these metals the transition is dependent on the protonation of Tyr188, rather than that of the Lys206-Lys296 dilysine bridge. Orders of metal free energies of binding relative to physiological Fe(III) were calculated, suggesting how well different metals can be transported

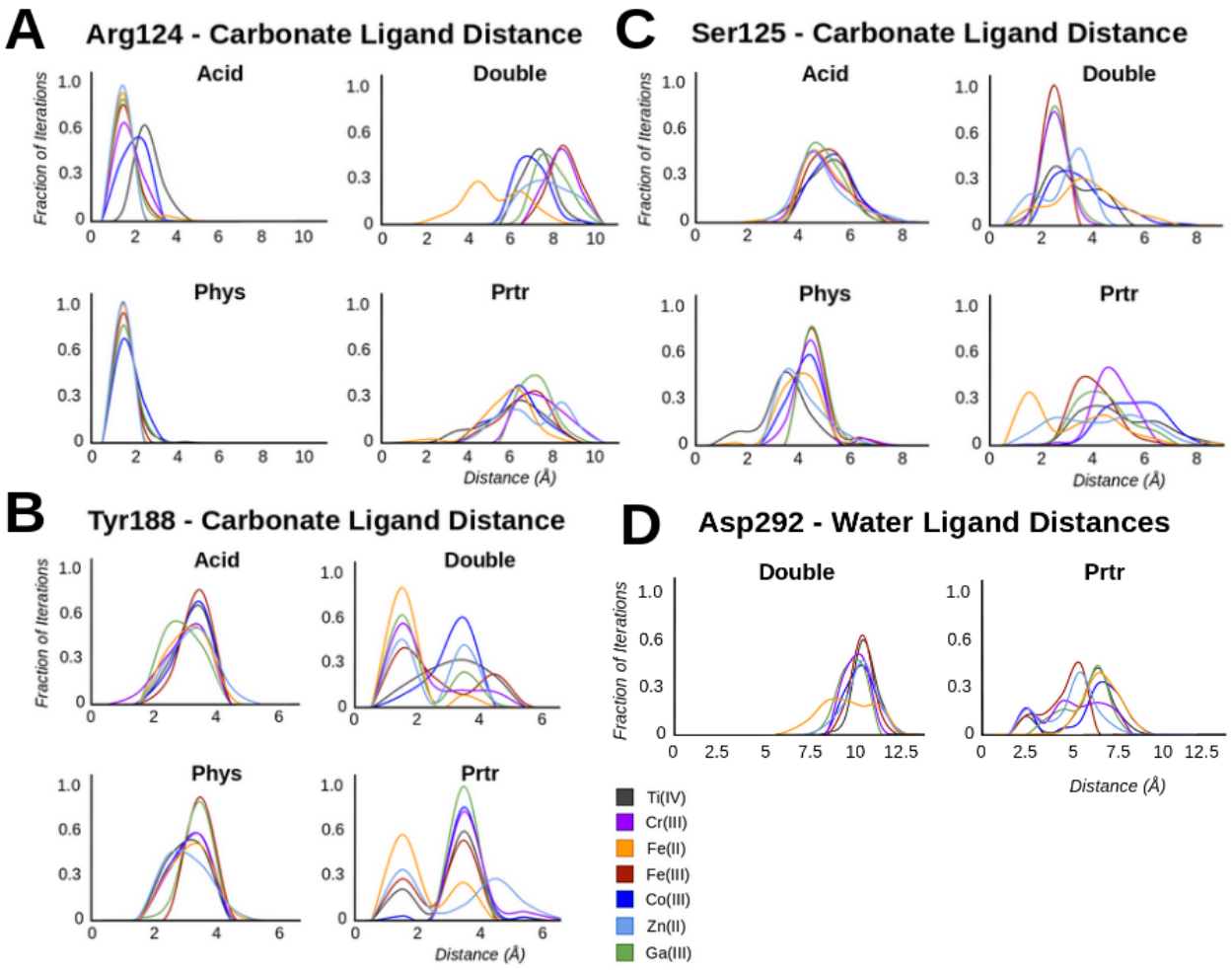

Figure 10: Histogram plots of critical interactions near the active site, sorted by metal and form of protein. The histograms are constructed of the interaction distances calculated for all iterations across all replicates for each state. Included here are plots of the (A) Arg124-carbonate distance and it replacements in the (B) Tyr188-carbonate distance and (C) Ser125-carbonate distance. The gating effect of Arg124 is clearly visible as the interaction begins consistent with a characteristic hydrogen bonding distance of about 2.5 Å in the closed Acid and Phys forms, but generally disappears to a greater distance in the Double and Prtr forms as hTF opens; both Ser125 and Tyr188 see the opposite trend, greatly preferring hydrogen-bonding distances in the open Double and Prtr forms of the protein. (D) The stabilizing interaction between Asp292 and the metal water ligand is only present in the Prtr form.

by hTF. The binding energies for the closed Phys form are consistent with experiment, while those for the open forms of the protein provide a unique, initial indication of hTF release preferences. Most importantly, the data from the Double form suggest that the root of Ti(IV) and Ga(III) cytotoxicity could arise from the difficulty by which they are released from hTF, which should be considered in future studies of their toxicity. Structural details of the simulations show that no single interaction explains the stability of the structure of the metal binding site, which instead arises from an aggregate of interactions largely about the active site. Given the central role of the synergistic anion, future research should focus on this moiety for the purposes of drug development and protein redesign. Also of interest is Asp292 and the loop it rests on, which could be used to target the Prtr state specifically through the unique interaction it makes with the metals ligands in that form. The simulations demonstrate throughout that the open Double and Prtr states of hTF are flexible in both active site interactions and protein conformation, while the closed Phys and Acid states are uniformly rigid. Ultimately, this study uncovered a nuanced network of interactions that could be modified to target hTF metal transport activity and address cytotoxic behavior.

Author Contributions

David J. Reilley and Michael R. Nechay devised the study. David J. Reilley, Jack T. Fuller, Michael R. Nechay, Marie Victor, Wei Li, and Josiah D. Ruberry ran simulations. David J. Reilley analyzed the data. Jon I. Mujika and Xabier Lopez provided consultation on the study. David J. Reilley, Jack T. Fuller, and Anastassia N. Alexandrova wrote the article.

Acknowledgement

The authors thank the Institute for Digital Research and Education at UCLA for supercomputer time. ANA thanks NSF for support with CAREER grant CHE-1903808. XL thanks MCIU/AEI/FEDER for financial support with Grant No. PGC2018-097529-B-100.

The authors also thank the students of Chem126, winter 2017 for setting up some of our simulations.

Supporting Information Available

An online supplement to this article can be found by visiting BJ Online at `http://www.biophysj.org`.

This material is available free of charge via the Internet at `http://pubs.acs.org/`.

References

1. Li, H., Sadler, P. J., and Sun, H. (1996) Rationalization of the strength of metal binding to human serum transferrin. *European journal of biochemistry 242*, 387–393.

2. Tinoco, A. D., and Valentine, A. M. (2005) Ti (IV) binds to human serum transferrin more tightly than does Fe (III). *Journal of the American Chemical Society 127*, 11218–11219.

3. Tinoco, A. D., Incarvito, C. D., and Valentine, A. M. (2007) Calorimetric, spectroscopic, and model studies provide insight into the transport of Ti (IV) by human serum transferrin. *Journal of the American Chemical Society 129*, 3444–3454.

4. Exley, C., Burgess, E., Day, J. P., Jeffery, E. H., and Yokel, R. A. (1996) Aluminum toxicokinetics. *Journal of Toxicology and Environmental Health Part A 48*, 569–584.

5. Exley, C. (2013) Human exposure to aluminium. *Environmental Science: Processes & Impacts 15*, 1807–1816.

6. Vera, J. L., Román, F. R., and Meléndez, E. (2004) Study of titanocene–DNA and molybdenocene–DNA interactions by inductively coupled plasma–atomic emission spectroscopy. *Analytical and bioanalytical chemistry 379*, 399–403.

7. Mokdsi, G., and Harding, M. M. (2001) Inhibition of human topoisomerase II by the antitumor metallocenes. *Journal of inorganic biochemistry 83*, 205–209.

8. Jakupec, M. A., and Keppler, B. K. (2004) Gallium in cancer treatment. *Current Topics in Medicinal Chemistry 4*, 1575–1583.

9. Cini, M., Bradshaw, T. D., and Woodward, S. (2017) Using titanium complexes to defeat cancer: the view from the shoulders of titans. *Chemical Society Reviews 46*, 1040–1051.

10. Sun, H., Li, H., and Sadler, P. J. (1999) Transferrin as a metal ion mediator. *Chemical reviews 99*, 2817–2842.

11. Li, H., and Qian, Z. M. (2002) Transferrin/transferrin receptor-mediated drug delivery. *Medicinal research reviews 22*, 225–250.

12. Gupta, Y., Jain, A., and Jain, S. K. (2007) Transferrin-conjugated solid lipid nanoparticles for enhanced delivery of quinine dihydrochloride to the brain. *Journal of pharmacy and pharmacology 59*, 935–940.

13. Lesley, J., Schulte, R., and Woods, J. (1989) Modulation of transferrin receptor expression and function by anti-transferrin receptor antibodies and antibody fragments. *Experimental cell research 182*, 215–233.

14. Ulbrich, K., Hekmatara, T., Herbert, E., and Kreuter, J. (2009) Transferrin-and transferrin-receptor-antibody-modified nanoparticles enable drug delivery across the blood–brain barrier (BBB). *European Journal of Pharmaceutics and Biopharmaceutics 71*, 251–256.

15. Huwyler, J., Wu, D., and Pardridge, W. M. (1996) Brain drug delivery of small molecules using immunoliposomes. *Proceedings of the National Academy of Sciences 93*, 14164–14169.

16. Noinaj, N., Easley, N. C., Oke, M., Mizuno, N., Gumbart, J., Boura, E., Steere, A. N., Zak, O., Aisen, P., Tajkhorshid, E., Evans, R. W., Gorringe, A. R., Mason, A. B., Steven, A. C., and Buchanan, S. K. (2012) Structural basis for iron piracy by pathogenic Neisseria. *Nature 483*, 53.

17. Dautry-Varsat, A., Ciechanover, A., and Lodish, H. F. (1983) pH and the recycling of transferrin during receptor-mediated endocytosis. *Proceedings of the National Academy of Sciences 80*, 2258–2262.

18. Sipe, D. M., and Murphy, R. F. (1991) Binding to cellular receptors results in increased iron release from transferrin at mildly acidic pH. *Journal of Biological Chemistry 266*, 8002–8007.

19. Grossman, J., Crawley, J., Strange, R., Patel, K., Murphy, L., Neu, M., Evans, R., and Hasnain, S. (1998) The nature of ligand-induced conformational change in transferrin in solution. *J. Mol. Biol. 279*, 461–472.

20. MacGillivray, R. T., Moore, S. A., Chen, J., Anderson, B. F., Baker, H., Luo, Y., Bewley, M., Smith, C. A., Murphy, M. E., Wang, Y., Mason, A. B., Woodworth, R. C., Brayer, G. D., and Baker, E. N. (1998) Two high-resolution crystal structures of the recombinant N-lobe of human transferrin reveal a structural change implicated in iron release. *Biochemistry 37*, 7919–7928.

21. Dhungana, S., Taboy, C. H., Zak, O., Larvie, M., Crumbliss, A. L., and Aisen, P. (2004) Redox properties of human transferrin bound to its receptor. *Biochemistry 43*, 205–209.

22. He, Q.-Y., Mason, A. B., Tam, B. M., MacGillivray, R. T., and Woodworth, R. C. (1999) Dual role of Lys206- Lys296 interaction in human transferrin N-lobe: Iron-release trigger and anion-binding site. *Biochemistry 38*, 9704–9711.

23. Steinlein, L. M., Ligman, C. M., Kessler, S., and Ikeda, R. A. (1998) Iron release is

reduced by mutations of lysines 206 and 296 in recombinant N-terminal half-transferrin. *Biochemistry 37*, 13696–13703.

24. Eckenroth, B. E., Steere, A. N., Chasteen, N. D., Everse, S. J., and Mason, A. B. (2011) How the binding of human transferrin primes the transferrin receptor potentiating iron release at endosomal pH. *Proceedings of the National Academy of Sciences 108*, 13089–13094.

25. Jeffrey, P. D., Bewley, M. C., MacGillivray, R. T., Mason, A. B., Woodworth, R. C., and Baker, E. N. (1998) Ligand-induced conformational change in transferrins: crystal structure of the open form of the N-terminal half-molecule of human transferrin. *Biochemistry 37*, 13978–13986.

26. Steere, A. N., Byrne, S. L., Chasteen, N. D., and Mason, A. B. (2012) Kinetics of iron release from transferrin bound to the transferrin receptor at endosomal pH. *Biochimica et Biophysica Acta (BBA)-General Subjects 1820*, 326–333.

27. Tinoco, A. D., Saxena, M., Sharma, S., Noinaj, N., Delgado, Y., Quinones Gonzalez, E. P., Conklin, S. E., Zambrana, N., Loza-Rosas, S. A., and Parks, T. B. (2016) Unusual synergism of transferrin and citrate in the regulation of Ti (IV) speciation, transport, and toxicity. *Journal of the American Chemical Society 138*, 5659–5665.

28. Curtin, J. P., Wang, M., Cheng, T., Jin, L., and Sun, H. (2018) The role of citrate, lactate and transferrin in determining titanium release from surgical devices into human serum. *JBIC Journal of Biological Inorganic Chemistry 23*, 471–480.

29. Baker, H. M., Nurizzo, D., Mason, A. B., and Baker, E. N. (2007) Structures of two mutants that probe the role in iron release of the dilysine pair in the N-lobe of human transferrin. *Acta Crystallographica Section D: Biological Crystallography 63*, 408–414.

30. Mujika, J. I., Escribano, B., Akhmatskaya, E., Ugalde, J. M., and Lopez, X. (2012)

Molecular dynamics simulations of iron- and aluminum-loaded serum transferrin: protonation of Tyr188 is necessary to prompt metal release. *Biochemistry 51*, 7017–27.

31. Rinaldo, D., and Field, M. J. (2003) A computational study of the open and closed forms of the N-lobe human serum transferrin apoprotein. *Biophysical journal 85*, 3485–3501.

32. Mujika, J. I., López, X., Rezabal, E., Castillo, R., Marti, S., Moliner, V., and Ugalde, J. M. (2011) A QM/MM study of the complexes formed by aluminum and iron with serum transferrin at neutral and acidic pH. *Journal of inorganic biochemistry 105*, 1446–1456.

33. Sparta, M., Shirvanyants, D., Ding, F., Dokholyan, N. V., and Alexandrova, A. N. (2012) Hybrid dynamics simulation engine for metalloproteins. *Biophysical Journal 103*, 767–776.

34. Ding, F., Tsao, D., Nie, H., and Dokholyan, N. V. (2008) Ab initio folding of proteins with all-atom discrete molecular dynamics. *Structure 16*, 1010–1018.

35. Nechay, M. R., Gallup, N. M., Morgenstern, A., Smith, Q. A., Eberhart, M. E., and Alexandrova, A. N. (2016) Histone deacetylase 8: Characterization of physiological divalent metal catalysis. *The Journal of Physical Chemistry B 120*, 5884–5895.

36. Valdez, C. E., and Alexandrova, A. N. (2012) Why urease is a di-nickel enzyme whereas the CcrA β-lactamase is a di-zinc enzyme. *The Journal of Physical Chemistry B 116*, 10649–10656.

37. Sparta, M., Valdez, C. E., and Alexandrova, A. N. (2013) Metal-dependent activity of Fe and Ni acireductone dioxygenases: how two electrons reroute the catalytic pathway. *Journal of molecular biology 425*, 3007–3018.

38. Valdez, C. E., Gallup, N. M., and Alexandrova, A. N. (2014) Co2+ acireductone dioxyge-

nase: Fe2+ mechanism, Ni2+ mechanism, or something else? *Chemical Physics Letters 604*, 77–82.

39. Nedd, S., Redler, R. L., Proctor, E. A., Dokholyan, N. V., and Alexandrova, A. N. (2014) Cu, Zn-superoxide dismutase without Zn is folded but catalytically inactive. *Journal of molecular biology 426*, 4112–4124.

40. Morgenstern, A., Jaszai, M., Eberhart, M. E., and Alexandrova, A. N. (2017) Quantified electrostatic preorganization in enzymes using the geometry of the electron charge density. *Chemical Science 8*, 5010–5018.

41. Valdez, C. E., Morgenstern, A., Eberhart, M. E., and Alexandrova, A. N. (2016) Predictive methods for computational metalloenzyme redesign-a test case with carboxypeptidase A. *Physical Chemistry Chemical Physics 18*, 31744–31756.

42. Reilley, D. J., Popov, K., Dokholyan, N. V., and Alexandrova, A. N. (2019) Uncovered Dynamic Coupling Resolves the Ambiguous Mechanism of Phenylalanine Hydroxylase Oxygen Binding. *The Journal of Physical Chemistry B*

43. Valdez, C. E., Sparta, M., and Alexandrova, A. N. (2012) The role of the flexible L43-S54 protein loop in the CcrA metallo-β-lactamase in binding structurally dissimilar β-lactam antibiotics. *Journal of chemical theory and computation 9*, 730–737.

44. Turbomole, V. 6.6; Turbomole Gmbh: Karlsruhe, Germany, 2014.

45. Staroverov, V. N., Scuseria, G. E., Tao, J., and Perdew, J. P. (2003) Comparative assessment of a new nonempirical density functional: molecules and hydrogen-bonded complexes. *The Journal of Chemical Physics 119*, 12129–12137.

46. Grimme, S., Antony, J., Ehrlich, S., and Krieg, H. (2010) A consistent and accurate ab initio parametrization of density functional dispersion correction (DFT-D) for the 94 elements H-Pu. *The Journal of Chemical Physics 132*, 154104.

47. Weigend, F., and Ahlrichs, R. (2005) Balanced basis sets of split valence, triple zeta valence and quadruple zeta valence quality for H to Rn: design and assessment of accuracy. *Physical Chemistry Chemical Physics 7*, 3297–3305.

48. Klamt, A. (1995) Conductor-like screening model for real solvents: a new approach to the quantitative calculation of solvation phenomena. *The Journal of Physical Chemistry 99*, 2224–2235.

49. Dojindo Molecular Technologies, I. Metal Chelates. Accessed: 2017-07-20.

50. Enesca, A., Isac, L., and Duta, A. (2015) Charge carriers injection in tandem semiconductors for dyes mineralization. *Applied Catalysis B: Environmental 162*, 352–363.

51. Marenich, A. V., Ho, J., Coote, M. L., Cramer, C. J., and Truhlar, D. G. (2014) Computational electrochemistry: prediction of liquid-phase reduction potentials. *Physical Chemistry Chemical Physics 16*, 15068–15106.

52. Sakajiri, T., Yajima, H., and Yamamura, T. (2012) Density Functional Theory Study on Metal-Binding Energies for Human Serum Transferrin-Metal Complexes. *ISRN Biophysics 2012*, 1–5.

Graphical TOC Entry